Internal Energy of Ions Generated by Matrix-Assisted Laser Desorption/Ionization

Guanghong Luo, Ioan Marginean, and Akos Vertes*

Department of Chemistry, George Washington University, Washington, D.C., 20052

To provide an objective measure of the correlation between the internal energy content of ions generated by matrix-assisted laser desorption/ionization (MALDI) and the matrix properties, a series of well-characterized benzyl-substituted benzylpyridinium salts were used as thermometer molecules (TMs). To determine the internal energy variations of analyte ions, the survival yields of TM molecular ions were measured in three different matrixes, α-cyano-4-hydroxycinnamic acid (CHCA), 3,5-dimethoxy-4-hydroxycinnamic acid (sinapinic acid, SA), and 2,5-dihydroxybenzoic acid (DHB). Statistical analysis of extensive survival yield data indicated that there were discernible differences among the studied matrixes. The experimental survival yields of the TM ions were used to calculate the unimolecular decomposition rate coefficient. Corresponding theoretical reaction rate coefficients were calculated based on the Rice−Ramsperger−Kassel−Marcus (RRKM) theory for different internal energies of the TMs. The internal energies of the ions were obtained by projecting the experimental rate coefficient values onto the theoretical curves obtained by the RRKM calculations. Molecular ions of the analytes showed decreasing survival yields and consequently increasing internal energies in the three matrixes in the following order: CHCA, SA, and DHB with "cold", "intermediate", and "hot" characteristics, respectively. Qualitatively, this could be interpreted as a significant departure from earlier observations suggesting an opposite trend. The classification as hot and cold matrixes should be further qualified by accounting for the influence of laser pulse energy and the nature of the analyte. Higher laser pulse energy led to an elevated level of energy transferred to the analyte, which in turn resulted in a diminished survival yield of the analyte molecular ion. It is quite possible that the assignment of hot and cold reverses as the analyte or the laser energy changes. These findings can help predict the outcome of postsource decay experiments and clarify the concept of hot and cold matrixes in MALDI mass spectrometry.

Since its introduction in the late 1980s, matrix-assisted laser desorption/ionization (MALDI) has become an increasingly significant technique in both biomolecular and macromolecular analysis.[1,2] Progress in the emerging field of proteomics clearly hinges on fast characterization of proteins and peptides, a task MALDI and electrospray ionization (ESI) mass spectrometry are uniquely positioned to perform.[3] Postsource decay experiments in MALDI are commonly utilized to gain primary structure as well as posttranslational modification data for peptides, information fundamental for protein identification.

Understanding ion production in MALDI can significantly contribute to the more efficient utilization of this method. Tasks ranging from matrix selection to fragmentation control might become rational steps in qualitative and potentially in quantitative analysis. There is considerable consensus over the mechanism of desorption initiated by UV irradiation,[4−7] but the ionization mechanism is still under debate.

An adequate ionization mechanism should be consistent with the thermodynamics of the process and should explain the presence and abundance of all the ions in the MALDI mass spectrum. At present, there is no single acceptable mechanism;[7,8] thus, the prediction of ion yields is very difficult if not impossible. It is expected that detailed analysis of the energetics involved can enhance our understanding of the ionization process.
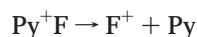
The internal energy of the molecular ions at generation determines the available fragmentation pathways. Due to experimental difficulties, there have been few reports on the internal energy of ions created by soft ionization methods, such as ESI and MALDI.[9,10] In a comprehensive paper, Vékey reviewed the effect of ion internal energies on mass spectra and the link between the internal energy of ions and the ionization mechanism of various ionization techniques.[11] The main methods to measure the internal energy of ions in mass spectrometry had been the thermometer molecule (TM) method,[12] the deconvolution method,[13]

(1) Tanaka, K.; Waki, H.; Ido, Y.; Akita, S.; Yoshida, Y.; Yoshida, T. *Rapid Commun. Mass Spectrom.* **1988**, *2*, 151.

(2) Hillenkamp, F.; Karas, M.; Beavis, R. C.; Chait, B. T. *Anal. Chem.* **1991**, *63*, 1193A−1201A.

(3) Godovac-Zimmermann, J.; Brown, L. R. *Mass Spectrom. Rev.* **2001**, *20*, 1−57.

(4) Vertes, A.; Gijbels, R.; Levine, R. D. *Rapid Commun. Mass Spectrom.* **1990**, *4*, 228−233.

(5) Vertes, A.; Levine, R. D. *Chem. Phys. Lett.* **1990**, *171*, 284−290.

(6) Vertes, A.; Irinyi, G.; Gijbels, R. *Anal. Chem.* **1993**, *65*, 2389−2393.

(7) Zenobi, R.; Knochenmuss, R. *Mass Spectrom. Rev.* **1998**, *17*, 337−366.

(8) Glückmann, M.; Pfenninger, A.; Krüger, R.; Thierolf, M.; Karas, M.; Horneffer, V.; Hillenkamp, F.; Strupat, K. *Int. J. Mass Spectrom.* **2001**, *210/211*, 121−132.

(9) Mowry, C. D.; Johnston, M. V. *J. Phys. Chem.* **1994**, *98*, 1904−1909.

(10) Stevenson, E.; Breuker, K.; Zenobi, R. *J. Mass Spectrom.* **2000**, *35*, 1035−1041.

(11) Vékey, K. *J. Mass Spectrom.* **1996**, *31*, 445−463.

* Corresponding author: (phone) 202-994-2717; (fax) 202-994-5873; (e-mail) vertes@gwu.edu.

and the survival yield method,[14] later refined to include the kinetic shift.[15]

The survival yield method, based on a series of TMs (benzyl-substituted benzylpyridinium salts), was utilized by De Pauw[15] for internal energy determination of ions generated by ESI. The rationale behind using this group of compounds lies with the simple fragmentation mechanism and with the well-studied thermodynamics of a wide range of N-alkylpyridinium cations.[18] The different substituents on the benzyl group result in different critical energies for the unimolecular decomposition reaction. The simple fragmentation pattern (the only analyte peaks observed in the mass spectrum correspond to the molecular ion, $M^+ = Py^+F$, and to the substituted benzyl cation fragment, F^+, produced by pyridine, Py, loss)

$$Py^+F \rightarrow F^+ + Py$$

enables the simple assessment of the decomposition of molecular ions. The survival yield of M^+

$$SY = \frac{I(M^+)}{I(F^+) + I(M^+)} \qquad (1)$$

in ESI was shown to depend on the internal energy of the TM.[14] In eq 1, $I(M^+)$ and $I(F^+)$ are the abundances corresponding to the molecular ion and the fragment ion, respectively.

Fragmentation close to the laser irradiance threshold for ion generation in MALDI can be viewed as a unimolecular decomposition reaction; thus, the experimental survival yields can be used to calculate the rate coefficients. These rate coefficients can also be calculated using the Rice−Ramsperger−Kassel−Marcus (RRKM) theory[18] for a particular internal energy of the ion. By projecting the experimental reaction coefficients on the RRKM curve, an estimate of the internal energy of the ions can be obtained. This method represents a simplification of the original survival yield method that has used additional assumptions on the functional form of the survival yield as a function of critical energy (see later).

There is only semiquantitative data available on the internal energy of ions in MALDI. In an early study, we compared the energy content of ions generated by direct laser desorption and MALDI using triphenylphosphonium salts as TMs.[19] Although reduced fragmentation in MALDI was clearly established, no quantitative measure for the ion internal energies was obtained. In this study, we extend the use of N-alkylpyridinium cations as TMs to characterize some of the most common MALDI matrixes

and determine the survival yield of analyte ions desorbed from a particular matrix at different laser pulse energies. This approach promises to provide a quantitative measure for the internal energy of MALDI generated ions. Correlations based on these data can be established between the internal energy, metastable decay, and fragmentation of molecular ions.

EXPERIMENTAL SECTION

Instrumentation. The molar absorptivity of the TMs at the laser wavelength was measured by a UV−visible spectrometer (UV-2401PC, Shimadzu Scientific Instruments, Inc., Columbia, MD). The time-of-flight mass spectrometer (TOF-MS) used in the MALDI experiments was a home-built linear instrument equipped with a nitrogen laser at 337 nm (VSL-337ND, Laser Science Inc., Newton, MA). A detailed description of this instrument can be found elsewhere.[20] The laser pulse energy was accurately adjusted by a variable attenuator (935-5-OPT, Newport, Fountain Valley, CA) and monitored by a pyroelectric joule meter (model J4-05, Molectron, Portland, OR). The laser beam was focused onto the probe tip at 45° to achieve $\sim 10^6$ W/cm² irradiance. The generated ions were extracted from the 1.0-cm-long accelerating region by 30.0 kV into the 2.15-m field-free drift region of the TOF-MS. A dual-microchannel plate assembly (30293, Galileo Electrooptics Corp., Sturbridge, MA) biased to 1700 V was used for the detection of ions. The signal was amplified by a fast preamplifier (9305, EG&G, Oak Ridge, TN) and recorded by a 1.5-GHz digital oscilloscope (LC684DXL, LeCroy, Chestnut Ridge, NY) at 500 Msamples/s sampling rate.

Materials. The matrixes, α-cyano-4-hydroxycinnamic acid (CHCA), 2,5-dihydroxybenzoic acid (DHB), and 3,5-dimethoxy-4-hydroxycinnamic acid (sinapinic acid, SA) were obtained from Sigma Chemical Co. (St. Louis, MO) and from Aldrich Chemical Co. (Milwaukee, WI), respectively. They were used without further purification. Acetonitrile solvent (HPLC grade) was purchased from Fisher Scientific (Springfield, NJ) whereas deionized water (18.2 MΩ·cm) was produced using an E-pure system (Barnstead, Dubuque, IA). All the benzyl-substituted benzylpyridinium chloride salts, 4-chloro- (4C), 4-floro- (4F), 4-methoxy- (4MO), 3-methoxy- (3MO), 4-methyl- (4M), 3-methyl- (3M), and 2-methyl- (2M), were custom synthesized by Celestial Specialty Chemicals (Nepean, Ontario, Canada). These chemicals were certified as reagent grade, and they were used without further processing.

Sample Preparation. Stock solutions of the analyte (5×10^{-4}−5×10^{-3} M) and the matrix (saturated) were prepared fresh daily by using 70% acetonitrile in deionized water. A 2-μL sample of analyte solution was mixed with 10 μL of matrix solution to obtain a matrix to analyte molar ratio of approximately 2000−3000. For most samples, 2 μL of this mixture was deposited on a stainless steel probe and air-dried at room temperature. The DHB samples were vacuum-dried using an evacuation chamber and a dual-stage rotary vane pump.

Data Acquisition and Processing. For each matrix−analyte combination, the minimum laser pulse energy that resulted in a fragment ion peak was determined. Then, each sample was analyzed at three to five laser pulse energies slightly above this value. Twenty spectra were acquired at each of 10 randomly

(12) Wysocki, V. H.; Kenttamaa, H. I.; Cooks, R. G. *Int. J. Mass Spectrom. Ion Processes* **1987**, *75*, 181−208.

(13) Vékey, K.; Brenton, A. G.; Beynon, J. H. *J. Phys. Chem.* **1986**, *90*, 0, 3569−3577.

(14) Derwa, F.; De Pauw, E. *Spectrosc. Int. J.* **1989**, *7*, 227−232.

(15) Collette, C.; Drahos, L.; De Pauw, E.; Vékey, K. *Rapid Commun. Mass Spectrom.* **1998**, *12*, 1673−1678.

(16) Derwa, F.; De Pauw, E.; Natalis, P. *Org. Mass Spectrom.* **1991**, *26*, 117−118.

(17) Katritzky, A. R.; Watson, C. H.; Dega-Szafran, Z.; Eyler, J. R. *J. Am. Chem. Soc.* **1990**, *112*, 2471−2478.

(18) Baer, T.; Mayer P. M. *J. Am. Soc. Mass Spectrom.* **1997**, *8*, 103−115.

(19) Claereboudt, J.; Claeys, M.; Geise, H.; Gijbels, R.; Vertes, A. *J. Am. Soc. Mass Spectrom.* **1993**, *4*, 798−812.

(20) Olumee, Z.; Sadeghi, M.; Tang, X.; Vertes, A. *Rapid Commun. Mass Spectrom.* **1995**, *9*, 744−752.
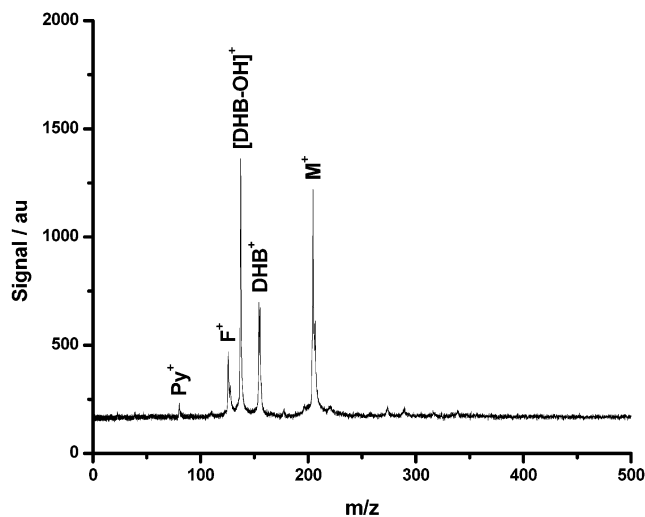
Figure 1. MALDI mass spectrum of 4C-benzylpyridinium chloride TM from DHB. Matrix ions are observed along with the molecular ions (M⁺) a single major fragment (F⁺), and a negligible amount of pyridinium ions (Py⁺) from the TM.
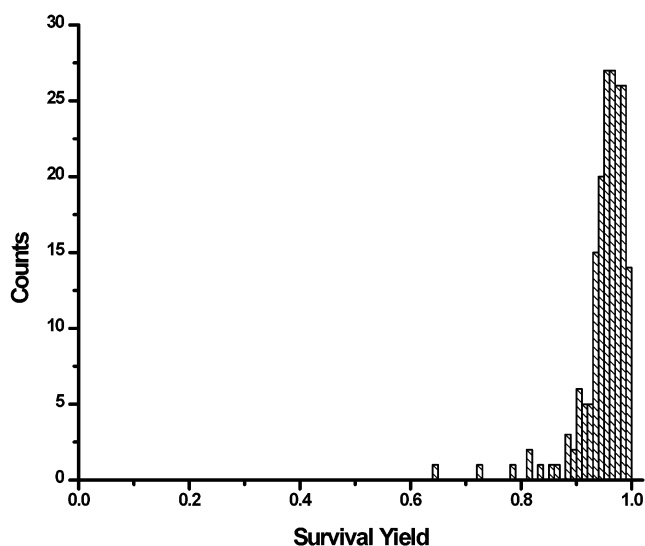

Figure 2. Histogram of survival yield data for 3MO-benzylpyridinium chloride ions desorbed from CHCA matrix. The data indicate that the average survival yield is a meaningful representation of the data set.

selected spots on the sample surface, resulting in a total of 200 spectra for every sample at every considered energy level. Figure 1 presents a mass spectrum collected for 4C-benzylpyridinium chloride in DHB. Data acquisition and processing were carried out on a PC using a homemade code in LabVIEW programming environment (National Instruments, Austin, TX). The ion current peaks corresponding to the molecular and fragment ions were integrated in time, and the experimental survival yields were calculated. To test the validity of this procedure, survival yield histograms were constructed for each sample. As demonstrated in Figure 2, the distribution of survival yields exhibited well-defined mean values.

According to the unimolecular kinetics valid for the ion source of a linear TOF-MS at low pressures, the survival yields were converted into experimental rate coefficients, $k_{exp}(E)$,

$$k_{exp} = -(1/\tau) \ln(\text{SY}) \tag{2}$$

Table 1. Molar Absorptivities of R-Benzylpyridinium Chlorides and Matrixes in Aqueous Solution at 337 nm

R	ϵ, L mol⁻¹ cm⁻¹	R	ϵ, L mol⁻¹ cm⁻¹	matrix	ϵ, L mol⁻¹ cm⁻¹
4-methyl-	0.000	4-chloro-	0.495	CHCA	17800
3-methyl-	0.113	3-methoxy-	8.55	SA	9170
4-floro-	0.210	4-methoxy-	40.9	DHB	3340
2-methyl-	0.431				

where τ is the reaction time in the accelerating region. The reaction time was selected as 100 ns for all TMs, an estimate supported by delayed extraction time values for small molecules on TOF-MS instruments as well as by plume dynamics calculations.[6]

Theoretical Calculations. The vibrational frequencies, needed in the RRKM rate coefficient calculations, were obtained from AM1 semiempirical molecular orbital calculations. The AM1 calculations were performed using PC Spartan version 1.3 (Wavefunction, Irvine, CA). The transition structure for each fragmentation reaction was determined by calculating the heat of formation (ΔH_f) of the ion for different configurations in which the reaction coordinate was constrained to different values (1.3–2.5 Å). The assumption was made that the reaction coordinate corresponds to the stretching of the C–N bond between the benzyl group and the pyridine ring.

Accounting for the vibrational degrees of freedom as harmonic oscillators, the classical RRKM rate coefficient, $k_{RRKM}(E)$, for unimolecular decomposition is

$$k_{RRKM}(E) = G^*(E - E_0)/h\rho(E) \tag{3}$$

where $G^*(E - E_0)$ is the total number of states between the E_0 and the E energy levels in the TS and $\rho(E)$ is the density of states at energy E for the reactant in EG (see, for example, ref 18). For the RRKM unimolecular decomposition rates of the TM ions, the Beyer–Swinehart direct count method was used to determine the density of states in EG and $\rho(E)$ and the number of states of the TS, $G^*(E - E_0)$ at a given internal energy, E.[18] The RRKM calculations were performed with a homemade program on a PC and tested against literature data on simple systems.[21]

RESULTS AND DISCUSSION

The laser energy is coupled into the sample through optical absorption. To demonstrate that energy is primarily deposited into the matrix molecules, we compared the relevant optical properties of matrixes and TMs. Molar absorptivities derived from the UV–visible spectra of these compounds are presented in Table 1. At the laser wavelength (337 nm), the optical absorption of the TMs was negligible compared to the matrix absorption. Although the spectra measured in solution may differ somewhat from the spectra of solid materials,[22] the large differences between the molar absorptivities of matrixes and TMs suggested that the laser light was predominantly absorbed by the matrix. The data in Table

(21) Drahos, L.; Vékey, K., *J. Mass Spectrom.* **2001**, *36*, 237−263.
(22) Allwood, D. A.; Dreyfus, R. W.; Perera, I. K.; Dyer, P. E. *Appl. Surf. Sci.* **1997**, *109/110*, 154−157.
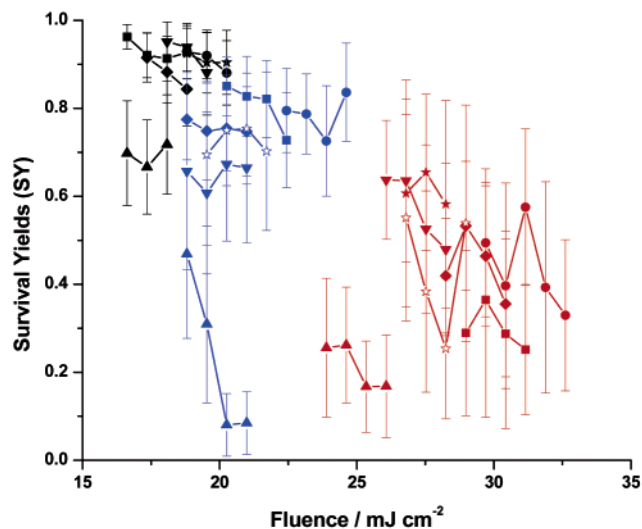
Figure 3. Survival yield results for substituted benzylpyridinium ions: 2M (■), 3M (●), 4M (♦), 3MO (▼), 4MO (▲), 4C (★), and 4F (☆) in matrixes CHCA (black), SA (blue), and DHB (red).

1 show that the lowest matrix-to-TM molar absorptivity ratio (in the case of DHB and 4MO) is ~80. Furthermore, the high matrix-to-TM molar ratio in MALDI samples makes light absorption by the matrix even more prevalent.

To differentiate direct laser desorption from MALDI, we studied the laser-induced mass spectra of neat TMs. The laser pulse energy needed for ion generation from neat TMs consistently exceeded the energy required for MALDI, e.g., by a factor of 2 for CHCA matrix. This observation was important because it proved that ion production in the survival yield experiments was indeed assisted by the matrix.

The next step was to prove that the choice of TMs was actually appropriate for monitoring the MALDI process. If there was no fragmentation observed or the fragmentation pattern did not change with experimental parameters, such as the selection of matrix or the laser pulse energy, the particular choice of TMs would have to be revised. Statistical analysis of extensive survival yield data indicated that TM fragmentation was consistently observed and there were discernible differences among the studied matrixes. Molecular ions of the analyte showed decreasing survival yields, indicating increasing internal energies in the three matrixes in the following order: CHCA, SA, and DHB (see Figure 3).

Changing the laser pulse energy indicated the presence of two MALDI thresholds for all three matrixes. At the first threshold (~10 mJ/cm² in CHCA matrix), the molecular ion of the TMs appeared in the spectra. At this point, the survival yield was equal to 1 as no TM fragment ions were observed. It is worth noting that at these pulse energies most of the time there were no matrix-related ions present. This can be viewed as an indication of preformed TM molecular ions in the solid. As the selected TMs are all salts, the appearance of preformed ions is quite fitting. At the second threshold (~15 mJ/cm² in CHCA), the fragment ion emerged and the survival yield declined from 1. As expected, further increase in laser pulse energy led to diminished survival yield of the analyte molecular ion. This was attributed to increased energy deposition into the matrix and an elevated level of energy transferred to the analyte. Figure 3 presents the survival yields

of the various TMs in CHCA, SA, and DHB versus the laser pulse energy above the second threshold.

To obtain a quantitative measure of the internal energy of the TMs, the survival yield data were converted to k_{exp} according to eq 2. Subsequently, the $k_{exp} = k_{RRKM}(E)$ equation was solved numerically for E to obtain the internal energy values. The determination of the $k_{RRKM}(E)$ based on eq 3 required information on the geometry, energetics, and vibrational frequencies of the EG and TS. The procedure described above is a simplified version of the survival yield method. There are two important changes. First, the internal energy is not represented by a distribution but by its average value. This simplification avoids having to make assumptions about the nature of the distribution (thermal vs nonthermal). As the laser excitation typically generates nonequilibrium internal energy distributions, this simplification also leads to a more reliable representation of the data. The other important difference is that we avoid the assumption of a sigmoidal relationship between E_0 and survival yield. This arbitrary hypothesis is used in the earlier versions of the survival yield method to obtain internal energy distributions (as opposed to the average value).[16]

To find the TS for the unimolecular decomposition of the TMs, AM1 calculations were carried out. Critical energies were obtained from refs 15 and 16. The vibrational frequencies for the studied TMs have been obtained by AM1 calculations and are provided as Supporting Information.

The 4MO compound also shows significantly lower values in the survival yields. This behavior could be attributed to direct energy deposition into this species from the laser (due to the larger molar absorptivity of this compound; see Table 1) or could be the consequence of the lower critical energy. For a given TM, lower E_0 leaves more energy available for the fragmentation reaction. Initial inspection of Figure 3 gives the impression that 4MO data does not fit with the rest of the data set. In the following analysis, it becomes obvious that this apparent discrepancy disappears when the survival yield data are converted into internal energies.

With the help of E_0 and vibrational frequencies for the EG and the TS, eq 3 was utilized to determine the RRKM rate coefficients as a function of internal energy. The results of the RRKM calculations for the seven TM ions are presented in Figure 4. Because of its structure and its low $E_{0,}$, for any given energy the rate coefficient for the unimolecular decomposition of 4MO is higher than that for the fragmentation of the other ions. At the other extreme, the 3MO ion has the lowest fragmentation rate coefficient for the relevant energies. The critical energy alone does not completely determine the rate coefficients. For example, the 4F shows lower $k_{RRKM}(E)$ values than 3MO at low energies, but it approaches roughly the same values at higher energies.

The experimental rate coefficients, k_{exp}, were calculated from the experimental survival yield values according to eq 2. Solving the $k_{exp} = k_{RRKM}(E)$ equation for E provided the internal energy values consistent with the survival yield data. These internal energies for all the TMs, matrixes, and laser energies are summarized in Figure 5. Looking at the average internal energy values found for the different matrixes, it is apparent that CHCA imparts the least amount of energy (3.69 ± 0.21 eV) on the TMs followed by SA (4.04±0.27 eV) and DHB (4.30 ± 0.29 eV). The corresponding confidence intervals for 95% probability are 0.45,
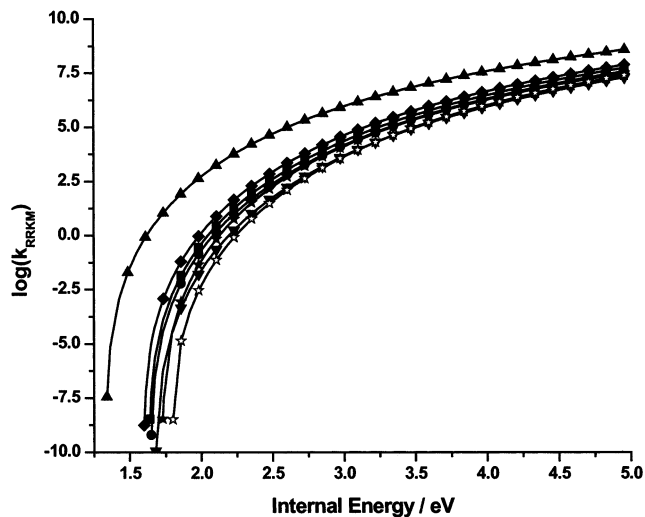
Figure 4. RRKM rate coefficients for substituted benzylpyridinium ions (2M (■), 3M (●), 4M (♦), 3MO (▼), 4MO (▲), 4C (★), and 4F (☆)) as a function of internal energy.
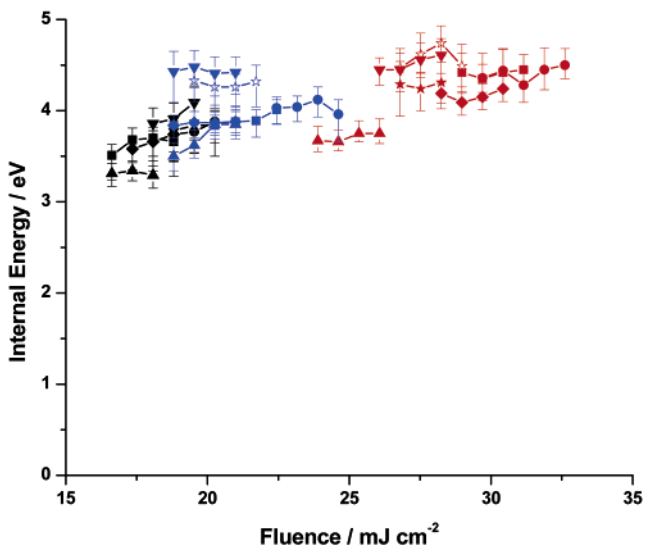

Figure 5. Internal energies of substituted benzylpyridinium ions (2M (■), 3M (●), 4M (♦), 3MO (▼), 4MO (▲), 4C (★) and 4F (☆)) in matrixes: CHCA (black), SA (blue) and DHB (red) as a function of laser pulse energy.

0.56, and 0.59 eV, respectively. This corresponds to a relative matrix assignment of cold, intermediate, and hot for CHCA, SA, and DHB, respectively.

Previous qualitative assignments of energy-transfer properties in MALDI were based on fragmentation patterns of small peptides.[23] In that study, however, laser pulse energy values were not provided. Qualitatively, our findings can be interpreted as a significant departure from these earlier data[23] asserting an opposite trend. It is true that, at similar laser energies, CHCA might seem "hotter" than SA or DHB, inducing more fragmentation in the analyte species. However, as has been demonstrated, the laser pulse energy cannot be neglected in assigning energy-transfer efficiency from matrix to analyte. Furthermore, the efficiency of energy transfer can also depend on the analyte. For example, the

role of preformed versus protonated ions should be further analyzed.

Analyzing the slopes in Figure 5, we found that in most cases the internal energy transferred to the analyte molecules increased as the laser pulse energy increased; i.e., the expected trend was confirmed. Although there was significant scatter in the rate of increase, differences could be established for the different matrixes. Comparing the average gains in internal energy for the three matrixes, one could discern that with the increase of laser energy the internal energy in CHCA grew faster than in the other two matrixes. In other words, while CHCA is the "coldest" matrix of the three, with increasing laser energy, it grows hotter faster than SA or DHB.

These observations in CHCA point to its unique behavior, which has been noted in the literature. This matrix is known to have the highest protonated molecular ion yield for glycine homologues[24] and lowest laser irradiance threshold for MALDI[25] among the three. One can argue that the lowest threshold value as well as being a relatively cold matrix are linked to the exceptionally high molar absorptivity for CHCA (at 337 nm, ~5 times higher than DHB; see Table 1). As the three matrixes have similar phase transition temperatures[10] (despite the differences in the hydrogen-bonding networks), the threshold energy for laser desorption is primarily governed by the light absorption properties. Because CHCA is capable of absorbing the laser light more efficiently, it can induce the desorption at lower laser energies. During the desorption process, the matrix molecules continue to absorb energy from the laser and transfer it to the analyte molecules. Because lower laser energy is available in the case of CHCA as compared to SA or DHB, the TM ions receive lower energy in this matrix through both direct absorption and non-radiative energy transfer. This scenario assumes that there are preformed ions in the sample. As demonstrated above, this is the case with the salts used as TMs; thus, ion yields are primarily determined by the release of ions from the solid. Furthermore, one can speculate that even in the case of neutral analytes enhanced matrix−analyte interaction can provide an efficient way of both transferring protons and communicating internal energy to the analyte molecules. Presumably, both of these processes take place through hydrogen-bonding networks.

The bottleneck model[4,5] can provide a partial explanation for the results. We can assume that the hydrogen bonds are mainly responsible for the interaction between the matrix molecules and the analyte molecules embedded in the matrix crystal. Each hydrogen bond provides a channel for energy transfer between the matrix and the analyte. The matrix that forms the most hydrogen bonds with the TMs would be able to transfer the energy most efficiently to the analyte and thus induce the highest degree of fragmentation. A simple count shows that each DHB molecule is able to form three hydrogen bonds, while CHCA and SA can only form two hydrogen bonds. This argument provides a qualitative explanation of why DHB can be viewed as the "hottest" among the three matrixes in this study. Although this argument may seem simplistic, a more in-depth look at the bottleneck model can reveal additional support for it. In ref 4, the effect of matrix absorption coefficients as well as the impact of

(23) Stimson, E.; Truong, O.; Richter, W. J.; Waterfield, M. D.; Burlingame, A. L. *Int. J. Mass Spectrom. Ion Processes* **1997**, *169/170*, 231−240.

(24) Olumee, Z.; Vertes, A. *J. Phys. Chem. B* **1998**, *102*, 6118−6122.
(25) Moskovets, E.; Vertes, A. *J. Phys. Chem. B* **2002**, *106*, 3301−3306.

vibrational frequency mismatch through the adiabaticity parameter is incorporated in the bottleneck model. Therefore, the increased internal energy of ions generated from DHB and the increased growth rate for the fluence dependence of the internal energy in CHCA are not necessarily in contradiction.

Comparing the fluorescence quantum efficiencies, φ_{qe}, of the three matrixes, however, we have found an interesting alternative explanation. Allwood and Dyer reported the fluorescence spectra, quantum efficiencies, and lifetime of several matrixes both in solution and in solid phase.[26] They found that in the solid phase φ_{qe}(DHB) = 0.59 and φ_{qe}(CHCA) = 0.082 and for SA fluorescence was below the detection limit. The remarkably high quantum efficiency in DHB opens up a new channel for energy transfer. As the fluorescence spectrum of this matrix covers the 375−550-nm range, it overlaps with the long-wavelength tail of the TM absorption spectra. This overlap can be the basis of off-resonance radiative energy transfer between DHB and TMs. It is clear from the significantly lower quantum yields of the other two matrixes that this mode of energy transfer is much less efficient and negligible for CHCA and SA, respectively. When present, radiative energy transfer in MALDI should be considered in competition with nonradiative channels.

CONCLUSIONS

This contribution, we believe, is the first report on internal energy measurements of analyte ions generated in MALDI experiments. We used a set of substituted benzylpyridinium salts as TMs to probe the energy transferred from the matrix to the analyte in the MALDI process. The calculations involved a simplified variant of the survival yield method combined with RRKM theory. We trust that a solid proof is provided for earlier conjectures that the internal energy deposited in the analyte during the MALDI process increases with the laser pulse energy.

Based on our findings, it is clear that the classification as hot and cold matrixes should be further qualified primarily by accounting for the influence of laser pulse energy. It is quite possible that the assignment of hot and cold reverses as the laser energy changes. Contrary to the currently accepted classification, we consider CHCA, SA, and DHB as cold, intermediate, and hot matrixes, respectively, at the laser pulse energies that induce fragmentation in TMs. Utilizing this understanding, postsource decay MALDI experiments, commonly used for peptide primary structure determination, can be better designed. Comparing fluorescence quantum efficiencies with our internal energy data, the observed correlation points to the need to further explore radiative energy transfer in MALDI.

SUPPORTING INFORMATION AVAILABLE

A listing (vibrational frequencies for the R-benzylpyridinium ions based on AM1 calculations). This material is available free of charge via the Internet at http://pubs.acs.org.

(26) Allwood, D. A.; Dyer, P. E., *Chem. Phys.* **2000**, *261*, 457−467.

Vibrational frequencies for the R-benzyl-pyridinium ions based on AM1 calculations

4C EG	4C TS	4F EG	4F TS	3MO EG	3MO TS	4MO EG	4MO TS	2M EG	2M TS	3M EG	3M TS	4M EG	4M TS
17	8	17	10	19	12	15	10	14	12	17	10	17	10
34	26	34	29	23	24	31	28	38	33	27	30	33	30
42	41	50	42	57	35	42	42	67	38	28	34	38	33
117	76	131	83	67	65	80	76	106	87	65	37	50	43
166	92	173	95	144	84	127	95	137	91	148	84	127	83
227	126	264	141	162	92	162	113	161	98	178	99	170	96
276	247	303	299	189	159	192	142	239	138	207	177	254	137
285	277	311	315	210	197	208	180	287	235	267	203	287	281
333	325	333	332	224	207	281	221	304	313	296	279	303	290
335	332	340	335	299	227	302	292	333	332	333	331	333	327
350	362	378	363	333	332	326	332	378	361	371	361	335	332
376	372	424	430	338	354	333	334	392	397	378	363	368	363
432	382	469	444	375	360	343	352	404	410	383	394	379	382
481	487	511	498	383	371	378	364	431	420	475	484	453	449
546	583	547	583	452	448	449	417	518	487	513	500	515	484
570	597	574	604	499	515	486	492	547	557	548	532	547	583
603	608	606	608	540	523	538	526	562	583	557	574	569	599
606	610	611	610	551	545	548	582	579	608	564	585	605	608
631	627	646	639	558	569	572	600	607	609	607	608	607	609
694	665	725	671	569	584	606	604	667	640	636	611	637	615
726	668	776	713	607	608	607	608	724	677	724	659	725	677
794	713	798	778	638	612	644	639	734	714	750	713	766	713
799	793	813	792	725	649	724	704	813	737	778	757	795	771
816	812	816	817	754	712	767	719	816	809	816	764	799	786
834	817	839	824	775	749	789	765	820	818	832	817	816	794
865	858	865	858	816	767	806	784	831	826	840	842	836	818
876	875	883	888	820	818	816	817	860	852	863	858	865	859
885	888	891	892	836	828	834	818	868	859	868	887	882	887
891	892	892	899	859	858	865	859	882	892	885	889	888	892
893	900	894	910	866	882	881	891	891	894	892	892	892	900
897	910	924	917	883	887	885	892	902	907	905	916	893	903
924	917	942	943	892	892	891	895	913	917	924	917	924	917
998	950	996	950	904	915	892	905	924	926	937	937	936	935
1020	991	1019	985	924	917	924	917	940	936	968	951	938	938
1038	1019	1038	1019	989	952	928	926	965	949	1001	971	967	949
1049	1033	1049	1033	1008	988	998	943	1019	960	1013	1006	1003	963
1061	1038	1055	1038	1021	1014	1019	987	1045	1019	1022	1012	1020	994
1068	1064	1068	1056	1043	1021	1042	1014	1049	1033	1041	1022	1039	1019
1070	1065	1070	1065	1049	1033	1049	1033	1063	1039	1050	1033	1050	1033
1110	1097	1102	1097	1050	1038	1049	1038	1068	1060	1068	1039	1063	1039
1114	1110	1126	1100	1063	1047	1062	1045	1070	1065	1070	1065	1068	1065

1127	1180	1173	1157	1068	1062	1068	1064	1074	1073	1072	1069	1070	1066
1174	1202	1176	1167	1070	1065	1070	1065	1083	1086	1095	1095	1110	1097
1180	1246	1186	1177	1093	1093	1098	1092	1129	1097	1126	1098	1127	1108
1203	1328	1212	1202	1103	1097	1117	1097	1175	1157	1136	1157	1171	1157
1226	1344	1232	1219	1127	1102	1127	1113	1177	1167	1174	1161	1179	1167
1248	1374	1254	1282	1161	1157	1168	1155	1186	1175	1178	1167	1184	1184
1249	1391	1257	1329	1176	1167	1174	1157	1219	1202	1205	1190	1207	1200
1256	1437	1264	1374	1178	1173	1190	1167	1227	1221	1227	1201	1229	1205
1305	1490	1392	1410	1198	1180	1193	1189	1236	1231	1234	1232	1232	1218
1395	1525	1399	1431	1214	1200	1215	1202	1247	1238	1240	1237	1237	1224
1397	1560	1407	1447	1226	1218	1224	1219	1254	1268	1255	1259	1255	1262
1439	1578	1440	1520	1229	1223	1229	1222	1260	1297	1256	1296	1256	1293
1456	1595	1516	1521	1241	1237	1240	1234	1269	1320	1263	1332	1262	1346
1573	2807	1568	1574	1255	1270	1256	1279	1294	1344	1294	1356	1294	1375
1576	2822	1574	1579	1257	1318	1263	1311	1317	1374	1343	1374	1364	1397
1577	2825	1576	1595	1277	1343	1288	1364	1396	1435	1396	1436	1396	1411
1586	2828	1600	2807	1309	1373	1306	1376	1426	1442	1438	1443	1404	1438
2662	2834	2662	2822	1371	1375	1395	1426	1440	1481	1449	1486	1440	1500
2718	2835	2718	2825	1396	1437	1403	1430	1484	1536	1471	1552	1492	1534
2771	2842	2771	2829	1439	1474	1418	1448	1574	1575	1575	1571	1575	1570
2790	2847	2790	2833	1459	1487	1440	1519	1577	1579	1577	1578	1577	1578
2831	2854	2831	2834	1493	1543	1507	1548	1584	1595	1586	1595	1584	1596
2840	2867	2840	2846	1575	1575	1575	1574	1599	2730	1599	2735	1596	2719
2848	2873	2848	2850	1576	1578	1577	1579	2658	2738	2663	2749	2664	2745
2850	2808	2853	2853	1586	1595	1582	1596	2714	2806	2719	2808	2719	2808
2851	2822	2855	2867	1596	2764	1591	2763	2735	2821	2737	2822	2734	2822
2860	2823	2861	2873	2664	2765	2664	2769	2747	2823	2751	2824	2751	2823
2864		2866		2719	2809	2719	2807	2765	2824	2767	2828	2768	2823
				2764	2823	2766	2822	2792	2828	2791	2831	2791	2828
				2766	2825	2767	2823	2831	2833	2832	2833	2831	2839
				2767	2829	2769	2826	2832	2839	2832	2840	2832	2840
				2790	2829	2792	2829	2841	2845	2841	2841	2841	2848
				2831	2833	2832	2837	2849	2854	2849	2852	2849	2852
				2832	2840	2833	2839	2850	2855	2852	2854	2854	2854
				2840	2849	2842	2853	2855	2867	2858	2868	2855	2868
				2849	2853	2850	2854	2858	2873	2860	2874	2862	2873
				2853	2854	2855	2859	2868		2868		2867	
				2862	2868	2857	2867						
				2868	2874	2866	2873						
				2872		2870							